Digital Signal Processing 50 (2016) 150–161

Contents lists available at ScienceDirect

Digital Signal Processing

www.elsevier.com/locate/dsp

Spectrally efficient emission mask shaping for OFDM cognitive radios

Thinh H. Pham [a], Suhaib A. Fahmy [b], Ian Vince McLoughlin [c,*]

[a] Faculty of Electrical and Electronics Engineering, Ho Chi Minh City University of Technology, Viet Nam
[b] School of Engineering, University of Warwick, UK
[c] School of Computing, University of Kent, UK

ARTICLE INFO

Article history:
Available online 29 December 2015

Keywords:
Cognitive radio
Software defined radio
OFDM
Inter-channel interference
IEEE 802.11

ABSTRACT

Orthogonal Frequency Division Multiplexing has been widely adopted in recent years due to its inherent spectral efficiency and robustness to impulsive noise and fading. For cognitive radio applications in particular, it can enable flexible and agile spectrum allocation, yet suffers from spectral leakage in the form of large side lobes, leading to inter-channel interference unless mitigated carefully. Hence, recent OFDM-based standards such as IEEE 802.11p for vehicular communication and IEEE 802.11af for TV whitespace reuse impose strict spectrum emission mask limits to combat adjacent channel interference. Stricter masks allow channels to operate closer together, improving spectral efficiency at the cost of implementation difficulty. Meeting these strict limits is a significant challenge for implementing both 802.11p and 802.11af, yet remains an important requirement for enabling cost-effective systems. This paper proposes a novel method that embeds baseband filtering within a cognitive radio architecture to meet the specification for the most stringent 802.11p and 802.11af masks, while allowing up to ten additional active 802.11af sub-carriers to occupy a single basic channel without violating SEM specifications. The proposed method, performed at baseband, relaxes otherwise strict RF filter requirements, allowing the RF subsystem to be implemented using much less stringent 802.11a designs, resulting in cost reductions.

1. Introduction and related work

Orthogonal Frequency Division Multiplexing (OFDM) has been adopted for many wireless standards as well as being an important enabling technology for cognitive radios. However, one of its main disadvantages is spectral leakage due to the summation of sinusoidal sub-carriers which are then widowed by a rectangular function. This has led to some recent OFDM-based standards demanding strict limitations on leakage into adjacent channels, in order to reduce inter-channel interference (ICI). In particular, this paper considers two such standards that impose strict limits on ICI; IEEE 802.11p, for Dedicated Short-Range Communications (DSRC) and IEEE 802.11af for cognitive radio access within television whitespace (TVWS) spectrum. This paper presents, discusses, implements, and evaluates a novel architecture capable of meeting the imposed adjacent channel interference limits defined by both OFDM standards.

1.1. 802.11p physical layer

In 2010, the IEEE defined the IEEE 802.11p standard for PHY and MAC layers [1], aimed at providing dedicated wireless links for new vehicular safety applications through vehicle-to-vehicle (V2V) and Road to Vehicle (RTV) communications. The IEEE 802.11p PHY was largely inherited from the well-established IEEE 802.11a OFDM PHY, with several modifications aimed at improving performance in vehicular environments. Basing the PHY on 802.11a reduces development efforts for 802.11p hardware and software, by enabling design re-use. It also allows backwards compatibility with 802.11a [2,3]. In essence, three main changes were made in moving from 802.11a to 802.11p:

1. A 10 MHz channel width instead of the 20 MHz in 802.11a. This extends the guard interval to address the effects of Doppler spread and inter-symbol interference inherent to vehicular communications.
2. Improved adjacent channel rejection performance in the receiver to reduce the effect of cross channel interference, again especially important in vehicular communication channels [4].

* Corresponding author.
E-mail address: ivm@kent.ac.uk (I.V. McLoughlin).

http://dx.doi.org/10.1016/j.dsp.2015.12.008
1051-2004/

3. Four spectral emission masks (SEMs) specified and mandated in FCC CFR47 Sections 90.377 and 95.1509. These class A to D specifications are all more stringent than those for current 802.11 radios.

In addition, 802.11p operates in the 5.9 GHz DSRC region which is divided into seven 10 MHz bands. This channelisation allows the MAC upper layer to perform multi-channel operations [5] and allows safety and other applications to occupy separate channels in order to manage and reduce interference. The four strict SEMs aim to reduce the effect of ICI between these channels although Wu et al. have shown that transmitters on adjacent service channels still cause ICI in the safety channel, even when they satisfy the class C requirement [6]. Shaping the 802.11p spectrum in order to reduce leakage and thus ICI is therefore important.

Thanks to the similarities between the two PHYs, some researchers have focused on adapting 802.11a PHY devices for 802.11p [7,8,2]. The transformation is typically accomplished in four parts, namely, reducing channel bandwidth, channel estimation, satisfying transmission power requirements, and ensuring effective channel access performance. Due to a dearth of affordable 802.11p prototype hardware, existing wireless testbeds for 802.11p tend to use modified 802.11a implementations [7]. For example, Almeda and Matos present a front-end using 802.11a hardware that is targeted to comply with 802.11p [9]. However, despite strict constraints, it does not meet the SEM requirements. Fuxjäger et al. similarly presented a transmitter implementation using the GNU Radio software-defined radio platform [10]. Despite being functional, the signal spectrum contained two peaks at image frequencies, which the output filter was unable to remove, and hence did not satisfy even the class A (most relaxed) SEM. Meanwhile, an early prototype transceiver based on a modified Atheros chipset [10], was able to fulfil class A requirements, but not classes C or D. It is clear that the stringent SEMs significantly increase the difficulty, and hence cost, of implementing new silicon or hardware for 802.11p. In fact, there has been much debate regarding whether and when chip makers will be able to meet such challenging requirements [4]. To the best of the authors' knowledge, no implementations or testbeds for 802.11p have been published that are able to meet the class D specification, prior to our own very recently published technique in [11].

1.2. 802.11af physical layer

In 2009, the FCC issued regulatory rulings for the reuse of television whitespace (TVWS) spectrum. In response, the 802.11 Working Group (WG) issued standard IEEE 802.11af to enable Wi-Fi in TVWS [12]. Continuing the theme of reuse, the standard defines amendments to existing high throughput 802.11ac PHY and MAC specifications to meet the requirements for channel access and coexistence in the TVWS region. Again, one of the main challenges is the stringent SEM requirement, which has been mandated by the FCC in the US and Ofcom in the UK. At present, a large gap exists between the spectral emissions of a scaled 802.11ac PHY and the mandated SEM for TVWS [13]. For instance, a (scaled) 802.11 implementation achieves an attenuation of 20 dB at the edge of the channel, whereas the requirement for portable TV band devices (TVBD) is 55 dB [14]. A working implementation was demonstrated by Lan et al. who presented the first prototype system of Wi-Fi in TVWS based on the 802.11af draft specification [14]. Their implementation achieved an attenuation of 35 dB at the edge of the channel, which is still far from meeting the required SEM.

1.3. Implementation

Modern OFDM implementations tend to favour subsuming as much processing as possible within the baseband digital components, in order to simplify the front-end RF hardware. Although many alternative transmitter designs exist, direct up-conversion (DUC) architectures are commonly selected due to inherent implementation, cost and performance advantages [15]. Within the transmitter, orthogonal intermediate frequency (IF) signals are generated directly by digital baseband hardware, high-pass filtered, and then quadrature up-converted to RF for transmission. This contrasts with more traditional digital radio implementations in which the digital hardware generates baseband signals which are up-converted to IF in one or more analogue steps before conversion to RF. Those systems would perform channel filtering predominantly with analogue filters, which require discrete precision components, and which tend to be inflexible in terms of carrier frequency and other characteristics. For cognitive radio (CR) systems, where frequency agility is a requirement, and in SDR (software defined radio), both up-conversion to IF as well as channelisation filtering are performed in the digital domain [16,17]. Typically, this enables a relaxation of stringent IF and RF filtering requirements, which in turn allows a reduction in system cost, though requiring more complex signal processing. A further advantage of baseband filtering is agility and flexibility. In a CR context in particular, both channel and time agility are required, and this can be best achieved in the digital domain.

Within the baseband, OFDM symbols are constructed in the frequency domain and then transformed to a complex time domain representation through the IFFT. A critically sampled construction process requires a sample rate of double the signal bandwidth. This signal is up-converted to IF using an interpolation process, during which images of the original OFDM frequency response are created at integer multiples of the original sampling rate. Image rejection filtering must then be performed on this signal prior to output by the digital-to-analogue converters (DACs) and subsequent transmission, since the images lie out-of-band (OOB) and hence are a cause of ICI.

However any such filtering induces time-domain smearing of the transmitted signals [18,19] which adds to the similar effects caused by the channel impulse response (CIR) between transmitter and receiver, all of which potentially induce inter-symbol interference (ISI).

OFDM systems combat ISI by dividing information finely in the frequency domain across sub-channels to implement narrow (in frequency) but long (in time) transmitted symbols, and then providing a guard interval between successive symbol blocks. The guard interval is determined by the duration of the expected channel and filter impulse responses that are traversed by each symbol on the path from transmitter baseband to receiver baseband. The guard interval typically contains a cyclic prefix (CP) which is inserted to combat another cause of ISI: received frequency components ringing during the CIR due to the abrupt onset of modulation at the beginning of each symbol. The nearly rectangular OFDM symbols in the time domain naturally have a frequency domain response consisting of overlapping sinc shapes, complete with large side lobes that lie outside the main frequency channel. These are another source of OOB interference which contributes to ICI. As noted previously, both 802.11p and 802.11af (in common with most OFDM-based standards) specify an SEM which requires that ICI is controlled.

In general there are two methods of achieving a given SEM. The first is to perform sharp filtering within the analogue RF transmission chain, while the second is to use digital baseband filtering techniques (which we have noted are generally considered to be advantageous in terms of flexibility, cost, design effort, size and component count). RF filtering methods were adopted in early SDR OFDM implementation like [17], and involve expensive hardware components such as oven-controlled crystal oscillators and precision passives, as well as adherence to tight design and

manufacturing rules. However the resulting systems are tuned to fixed frequency bands, and thus unsuited to the required frequency agility of CR systems which must switch between different regions of the frequency spectrum. Thus, addressing the challenge of meeting SEM requirements through baseband processing in CR systems is both sensible and practical. As an example, we recently demonstrated the first baseband digital filtering method capable of meeting the 802.11p Class D SEM [11].

Digital methods can be classified into either frequency or time domain techniques. The former are effective but are highly complex [20] and will not be considered further in this paper. The latter techniques are dominated by shaping methods [21,22], which apply a time domain window to the OFDM symbol to modify its response in the frequency domain prior to up-conversion, as applied in [11].

1.4. Dynamic channel requirements

For static wireless devices operating in licensed spectral regions, the characteristics of communication systems that are licensed to occupy adjacent bands may be known. Hence, spectral leakage masks for ICI avoidance in neighbouring systems can be statically specified. However, in the case of shared and reused spectrum, the authors of [23] suggest that SEMs should be defined in a more general and flexible way. In other words, CRs operating in dynamic spectrum access (DSA) environments must adapt their current transmission SEMs based upon their current operating region – another argument for baseband digital filtering. More sophisticated examples of SEMs are studied in [24], which deals with the broader concept of dynamic SEMs.

Time-varying SEMs may also need to consider that neighbouring systems are themselves able to change their SEMs, and hence, through negotiation with each other, change their masks for in- and out-of-band emission levels separately in accordance with their mutual temporal variations (for example, to adapt to communication traffic density or spatial deployment density). In such future systems, an SEM defined by the regulator may simply be a starting point in a collaborative process in which neighbouring communication systems negotiate and renegotiate new SEMs as their statuses change (e.g. to optimise computational power or increasing throughput).

Unfortunately, the authors in [24] did not present a complete solution for dynamic filtering of spectral emissions, however they discussed deactivating sub-carriers or changing transmission power to satisfy the requirements of a dynamic SEM. The former solution leads to a reduction in throughput due to reduced spectral band occupancy, whereas the latter impacts range. A combined approach was presented in [25] where some sub-carriers are reduced in power instead of being deactivated, in order to reduce leakage into adjacent channels.

1.5. Contributions

The first contribution of this paper is to define a CR signal processing architecture for SDR that performs a flexible degree of spectral shaping, at an adaptable rate, in the digital baseband. This adopts the novel baseband filtering technique proposed in [11], extended to support not only channel and time agility, but also to reduce the degree of shaping for conditions where transmission power is reduced. The second contribution is to evaluate the technique for both 802.11p and 802.11af spectral shaping. For each standard, the proposed signal processing approach is shown capable of meeting the very strict adjacent channel interference limits. This includes 802.11af in the TVWS, as well as the most stringent SEM for 802.11p. This is the first shaping method, to the authors' knowledge, that can meet the most challenging SEM requirements for both standards. In addition, we have implemented the signal processing algorithms within a CR framework using reconfigurable logic. A third contribution is to demonstrate the feasibility of selective sub-carrier deactivation and reactivation to maximise spectral efficiency in the face of changing transmission power requirements.

The remainder of this paper is organised as follows. Section 2 presents an OFDM signal model which accounts for the channel-related parameters of both 802.11p and 802.11af. Section 3 discusses existing pulse shaping approaches for reducing spectral leakage in OFDM-based systems in general, before identifying potential methods to be evaluated for either 802.11p or 802.11af. Section 4 then presents the proposed method, applies it first to the stringent 802.11p SEM specification and then to that for 802.11af, before discussing overall performance and opportunities for increasing spectral efficiency. Conclusions and future work are presented in Section 5.

2. Signal model

We define an OFDM symbol to have inverse fast Fourier transform (IFFT) length and cyclic prefix (CP) length N and N_{CP}, respectively, so that the length of the symbol including its CP is $N_T = N + N_{CP}$. A sample $x(m)$ of the OFDM symbol $(0 \leq m \leq N_T - 1)$ can be expressed in the time domain as

$$x(m) = \frac{1}{N} \sum_{k=0}^{N-1} X(k) e^{i2\pi \frac{k}{N}(m-N_{CP})}, \tag{1}$$

where $X(k)$ denotes the frequency domain representation of the data sub-carriers. Since OFDM symbol samples are generally transmitted sequentially, this is equivalent to multiplying symbols with a rectangular window function, p. Then the transmitted OFDM samples can be expressed as

$$x(n) = \frac{1}{N} \sum_{l=-\infty}^{\infty} \sum_{k=0}^{N-1} X(k) p(n - lN_T) e^{i2\pi \frac{k}{N}(n-N_{CP}-lN_T)}. \tag{2}$$

In a conventional OFDM system, the window function $p(m)$ is rectangular, described as

$$p(m) = \begin{cases} 1, & m = 0, 1, \ldots, N_T \\ 0, & otherwise \end{cases} \tag{3}$$

The CIR, of length h, is derived from the delay spread of the channel. If the CP is shorter than the channel delay, ISI will be present in received symbols. Channels experienced by the two standards discussed in this paper will obviously differ, but both tend to experience high levels of delay spread: 802.11p because it is primarily a vehicular communications standard, and 802.11af because it operates in lower attenuation UHF and VHF bands.

As mentioned in Section 1, the PHYs specified in 802.11p and 802.11af are largely inherited from the well-established 802.11a and 802.11ac OFDM PHYs, respectively. The major parameters of both new PHYs are presented in Table 1. However, since the new standards operate in different channel regions and environments, they are subject to different, and much more stringent SEM requirements than their parent standards.

2.1. 802.11p signal and channel models

802.11p is defined for vehicular channels that tends to experience a larger delay spread than WLAN. While the 802.11p symbol has 16 samples for CP (i.e. the same as in 802.11a), the guard intervals are lengthened to avoid ISI by reducing the bandwidth from

Table 1
Major parameters of 802.11p and 802.11af OFDM PHYs.

Parameters	802.11p	802.11af		
Bandwidth, MHz	10	6	7	8
Used subcarriers, N_C	52	114		
Total subcarriers, N_T	64	144	168	144
FFT points, N_{FFT}	64	128		
Subcarrier spacing Δf, MHz	10/64	6/144	7/168	8/144
Sampling frequency, MHz	10	5.33	5.33	7.11
Fourier transform length, μs	6.4	24	24	18
CP length, μs	1.6	6	6	4.5

20 MHz to 10 MHz (i.e., a 10 MHz sampling frequency). However this raises some challenges in the frequency domain. First, reducing bandwidth requires a higher quality factor front-end filter circuit for the higher frequency carrier compared to 802.11a. Second, 802.11p shares a 6 sub-carrier spacing frequency guard per side with 802.11a. Given the reduced sampling frequency, this leads to the absolute frequency guard being correspondingly narrower.

Generally, vehicular communication channels with large delay spread will require an increased timing guard, hence narrowing the frequency guard, which leads to stricter filtering constraints. Empirical channel models in [26,27] reveal how maximum delay spread varies depending on different propagation models and traffic environments. For example, the RTV model for suburban street, urban canyon, and expressway have maximum excess delays of 700, 501, and 401 ns, respectively [26]. For the V2V model, measurements in [27] reveal that the 90% largest delay spread (found in urban areas) is near 600 ns, which is equivalent to 6 samples. Given the fact that the CP is 16 samples, this leaves 10 samples (1 μs) remaining. Any spectral leakage filtering necessary to meet the stringent SEM specification must not encroach further than this into the guard time.

2.2. 802.11af signal and channel models

On the other hand, 802.11af is defined to reuse white space in the UHF band, with three basic channel units (BCUs) of 6 MHz, 7 MHz, and 8 MHz. Within this paper, we will confine our consideration to the narrowest (and hence possibly most problematic) 6 MHz BCU for investigating the performance of the proposed filtering method for 802.11af.

In the 802.11af channel, the measured delay spread is less than 1 μs [14], which is equivalent to the duration of 6 samples in the CP. Therefore, the 802.11af guard interval of 6 μs is sufficient to avoid ISI, with the remaining 5 μs (i.e., 26 samples) being available for filtering spectral leakage, if necessary. In the US, FCC rules mandate a very strict SEM to avoid ICI on the adjacent channels of primary users in the UHF band. For 6 MHz channels, the signal transmitted by TVBDs shall maintain at least 55 dB attenuation at the edge of the channel, which is significantly higher than the requirement of the parent 802.11ac standard. In the UK, the Ofcom requirement for 8 MHz channels is similarly strict.

3. State of the art spectral leakage filtering

To the best of the authors' knowledge, no baseband filtering solution has yet been published which has been shown to meet the strict SEM criteria for both 802.11p and 802.11af. However, several methods have been shown to be effective at mitigating spectral leakage for the less stringent parent standards 802.11a, and 802.11ac.

This section investigates state of the art methods for 802.11a and 802.11ac, and considers their application for the newer standards. Specifically, each method is evaluated, and shown to be unsuitable for meeting the strict SEM criteria for 802.11p (and hence very unlikely to satisfy the even more stringent 802.11af SEM).

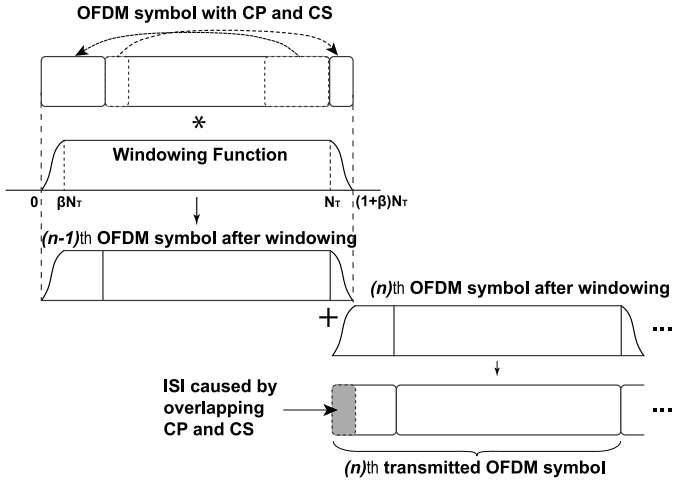

Fig. 1. Pulse Shaping operation performed on OFDM symbols.

3.1. Pulse shaping

Pulse shaping (using a smooth rather than rectangular pulse), recommended in 802.11a, is effective at reducing side lobes, although it induces distortion in the subcarriers. One way to avoid the distortion is to add extending parts, i.e. CP and cyclic suffix (CS), concatenated to the conventional OFDM symbol before the beginning and after the end respectively. The extended symbol is then multiplied with a smoothing function. While the CP in conventional OFDM is used as a guard interval, here it is also occupied, along with the CS, for pulse shaping.

Pulse shaping extends the N_T length of the OFDM signal by a roll-off factor, β. One effect of extending the symbol is to reduce spectral efficiency, and thus the CP and CS of consecutive symbols can be overlapped, as shown in Fig. 1. This, in turn, causes ISI in the overlapped region.

In practical terms, pulse shaping using the overlapping method effectively shortens the OFDM guard interval. A larger β means reduced spectral leakage, at the cost of reducing the effective guard interval since a number of guard interval samples are consumed for pulse shaping. If βN_T is increased to equal the CP length, the effective guard interval is reduced to zero (i.e. there is no guard interval to prevent channel-induced ISI). In this paper, three state-of-the-art smoothing functions for pulse shaping are investigated. We present each in discrete form, before investigating their performance with different roll-off factors. The first smoothing function, denoted p_1, is present in the IEEE 802.11a standard:

$$p_1(m) = \begin{cases} sin^2(\frac{\pi}{2}(0.5 + \frac{m}{\beta N_T})), & -\frac{\beta N_T}{2} \le m < \frac{\beta N_T}{2} \\ 1, & \frac{\beta N_T}{2} \le m < N_T - \frac{\beta N_T}{2} \\ sin^2(\frac{\pi}{2}(0.5 - \frac{m-N_T}{\beta N_T})), & N_T - \frac{\beta N_T}{2} \le m < N_T + \frac{\beta N_T}{2} \end{cases} \quad (4)$$

The second, proposed by Bala et al. [28], is based on a raised cosine function, denoted here as p_2:

$$p_2(m) = \begin{cases} \frac{1}{2} + \frac{1}{2}cos(\pi(1 + \frac{m}{\beta N_T})), & 0 \le m < \beta N_T \\ 1, & \beta N_T \le m < N_T \\ \frac{1}{2} + \frac{1}{2}cos(\pi(\frac{m-N_T}{\beta N_T})), & N_T \le m < (1+\beta)N_T \end{cases} \quad (5)$$

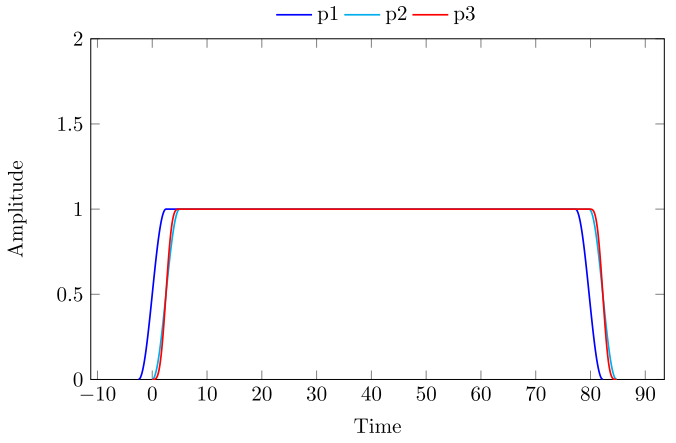

Fig. 2. The shapes of the considered window pulses. (For interpretation of the colours in this figure, the reader is referred to the web version of this article.)

The third, denoted p_3, is based on the characteristics of functions with vestigial symmetry as derived by Castanheira and Gameiro [29]:

$$p_3(m) = \begin{cases} \frac{1}{2} + \frac{9}{16}cos(\pi(1 - \frac{m}{\beta N_T})) \\ -\frac{1}{16}cos(3\pi(1 - \frac{m}{\beta N_T})), & 0 \le m < \beta N_T \\ 1, & \beta N_T \le m < N_T \\ \frac{1}{2} + \frac{9}{16}cos(\pi\frac{m-N_T}{\beta N_T}) \\ -\frac{1}{16}cos(3\pi\frac{m-N_T}{\beta N_T}), & N_T \le m < (1+\beta)N_T \end{cases} \quad (6)$$

The compression of OFDM spectral side lobes as a consequence of pulse shaping is investigated by first assuming that the effect of the image spectrum caused by interpolation or digital-to-analogue conversion (DAC) is negligible. This assumption is noted because the band gap between the desired spectrum and its image is relatively narrow. Thus the overlapping image spectrum can influence the effectiveness of the shaped spectral leakage. The issue will be discussed later in the paper, where image cancellation is presented separately for 802.11p and 802.11af.

Fig. 2 illustrates the shapes of the different smoothing functions mentioned above. Note that both p_1 and p_2 are derived from raised cosines, and thus have identical shape but are shifted in the time domain. Smoothing functions p_2 and p_3 are simulated for otherwise identical channels and signals, and compared in Fig. 3, which reveals the spectral envelope attenuation for the different smoothing functions with various roll-off factors. Class C and D emission mask limits are overlaid on the plot. For example, lines marked $p_2\_\beta 1$, $p_3\_\beta 1$ plot the OFDM signal spectra for smoothing functions $p_2(m)$ and $p_3(m)$, respectively, and roll-off factor $\beta N_T = 1$. Roll-off factors of $\beta N_T = 5$ and $\beta N_T = 7$ are also plotted in Fig. 3 along with *os*, the original OFDM spectrum without any pulse shaping applied.

In the case of using one guard interval sample, the spectral leakage is reduced slightly compared to the original OFDM signal. The shaped spectra do not meet the emission requirement of class C. When 5 CP samples and 7 CP samples are used for pulse shaping, $p_2(m)$ and $p_3(m)$ achieve a significant improvement. $p_2(m)$ obtains better results compared to $p_3(m)$ and in fact, $p_2\_\beta 5$ satisfies class C and almost meets the requirement of class D.

Thus, we can state that, ignoring the presence of an image spectrum as noted previously, the pulse shaping method can use part of the guard interval to apply a smoothing function in order to shape the spectral leakage and nearly meet stringent SEM requirements.

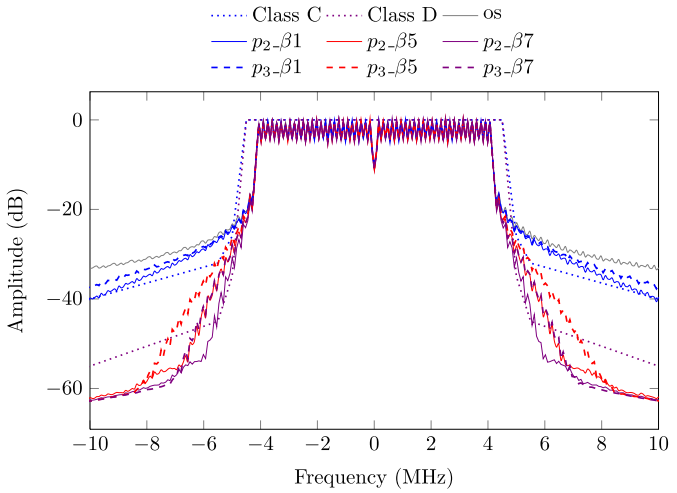

Fig. 3. Spectral envelope due to pulse shaping OFDM symbols using the smoothing functions and different roll-off factors for 802.11p. Class C and D spectral emission mask limits are overlaid as dotted lines. (For interpretation of the colours in this figure, the reader is referred to the web version of this article.)

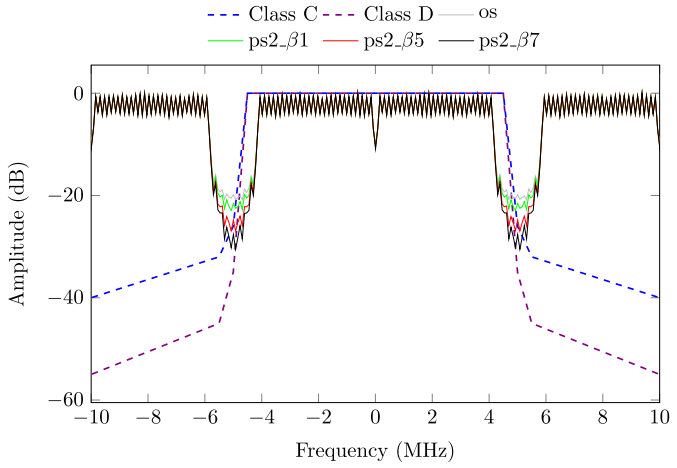

Fig. 4. Spectrum of 802.11p OFDM symbols shaped with different window functions, with the image spectrum included. (For interpretation of the colours in this figure, the reader is referred to the web version of this article.)

To investigate further, the spectral shaping including the presence of the image spectrum – a consequence of the interpolation – is shown in Fig. 4. Apart from the original spectrum, *os*, results are shown for $p_2(m)$ pulse shaped 802.11p OFDM symbols. Clearly, pulse shaping yields a response that is similar to, but slightly better than, the original OFDM signal. However, when the image spectrum is considered, pulse shaping cannot achieve meaningful adjacent channel signal compression because the band gap between the main spectrum and image spectrum is insufficient for pulse shaping to achieve any significant spectral attenuation. The other smoothing functions achieve similar results but are not plotted here for reasons of space.

In a practical system, the consequence is that almost all of the side-lobe attenuation may need to be contributed by sharp and hence both high order and accurate analogue filters. Such filters contribute design complexity, increased component count, manufacturing difficulty, and additional cost to a product.

3.2. Image spectrum cancellation by FIR filter

The critical issue for 802.11p signals to meet the stringent mask requirements is that the frequency guards are narrow and the car-

Table 2
Popular window-based FIR filter lengths.

Window	Stopband attenuation	Filter length, N	Length for 802.11p
Hamming, *HM*	−26.5 dB	$\frac{6.22\pi}{\Delta\omega}$	$N \approx 31L$
Hanning, *HN*	−31.5 dB	$\frac{6.65\pi}{\Delta\omega}$	$N \approx 33L$
Blackman, *BM*	−42.7 dB	$\frac{11.1\pi}{\Delta\omega}$	$N \approx 55L$
Kaiser, *KS*	–	$\frac{A-7.95}{2.23\Delta\omega}$, $A > 21$	$N \approx 33L$
		$\frac{5.79}{\Delta\omega}$, $A < 21$	
Chebyshev, *CW*	–	$\frac{2.06A-16.5}{2.29\Delta\omega}$	$N \approx 67L$

rier frequency is relatively high (5.9 GHz) compared to 802.11a. Similarly, the 802.11af guard bands are even narrower, and the sub-channels are also much narrower. Interpolation can be used at baseband to increase sampling frequency, and thereby expand the baseband bandwidth. This then provides a wider frequency transition band, which is easier to fit a filter roll-off response into, however the resulting image spectra (repeats of the original baseband spectrum, as mentioned in Section 1.3) must then be removed by filtering. Such filters are commonly implemented using finite impulse response (FIR) form filters. A cascaded integrator comb (CIC) implementation is sometimes chosen, since this can combine the interpolation and filtering steps, however while it is computationally efficient it lacks flexibility, Since this paper is concerned with the tradeoff between the filter order, duration of impulse response, degree of oversampling, and filter transition band sharpness, flexibility is important and thus general FIR form filters are assumed.

The tradeoff mentioned above exists because the narrow band gap between main and adjacent image spectra mandates a high order filter to remove ICI, which generally implies a high order and thus long impulse response filter. Unfortunately the long impulse response of the filter has a similar effect to the impulse response of the overall channel in terms of inducing ISI. Thus the FIR filter also reduces the effective guard interval of OFDM symbols [30]. Consequently, its design must contribute to the wider tradeoff between ISI avoidance, spectral efficiency (the transition band width), and the degree of filter attenuation needed to meet the SEM requirement.

Several widely used FIR implementation filters are listed in Table 2. These are all investigated for image spectrum attenuation, as applied to 802.11p symbols initially, and then evaluated for 802.11af. An empirical formula [31] is used to estimate the length of each filter in terms of attenuation A and transition band $\Delta\omega$. The specifications of the stringent 802.11p class D SEM are used to calculate the required number of taps with L-fold interpolation, in terms of L.

It is noticeable that the required lengths of these FIR filters for 802.11p are all longer than the 1.6 µs guard interval of the 802.11p symbol. For example, the Hanning window requires filter length $N \approx 33 \times L$ samples, equivalent to a duration of 3.3 µs. To avoid ISI, the maximum length of the FIR filter is derived by taking into account the guard interval and the CIR. By assuming that the delay spread of the vehicular channel is constrained to a maximum of 600 ns (as discussed in Section 2) based on the results stated in [26,27], the CIR is equivalent to 6 samples of the 802.11p guard interval (the sampling frequency of 802.11p is 10 MHz). Therefore, a remaining effective guard interval of 10 samples is available for filtering. However, when the filter is used in a transmitter, a matched filter is required at the receiver [30] with equivalent length, meaning that the remaining guard interval is effectively halved: only 5 samples remain for transmitter filtering.

Given that L-fold interpolation is used at the transmitter, the permitted FIR filter length becomes $5 \times L$, constituting one of the rules for the FIR filter design process.

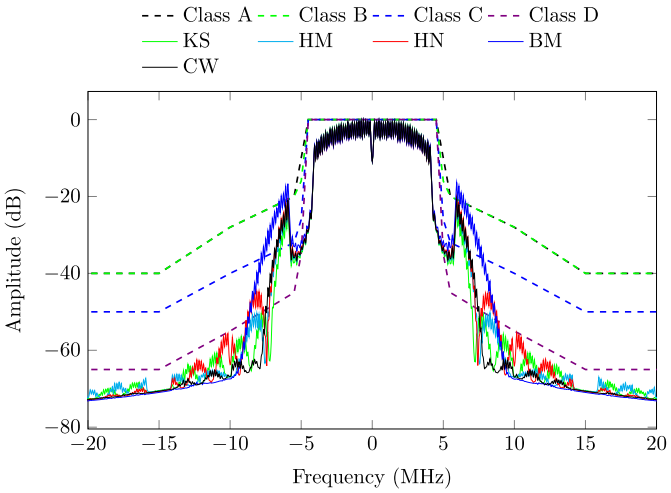

Fig. 5. Spectra of OFDM symbols for 802.11p using different FIR interpolation filters, with $L = 8$. (For interpretation of the colours in this figure, the reader is referred to the web version of this article.)

Theoretically, in the conventional approach, a value of L can be chosen based on the baseband sampling frequency ($F_s = 10$ MHz for 802.11p) and the DAC maximum frequency, F_{DAC}^{max}, such that $F_{DAC} = L.F_s \leq F_{DAC}^{max}$.

In the proposed method, the baseband frequency of the OFDM symbol is increased by a factor of M over the critical sampling frequency (where M is a power of two). Thus, to maintain the same DAC sampling frequency, $F_{DAC} = L' \cdot M \cdot Fs$, only L'-fold interpolation is required. It is clearly preferable that L'/M is an integer. For comparison between the proposed and conventional approaches, L should also be an integer, and in this paper, assuming $F_{DAC}^{max} = 80$ MHz, we choose $L = 8$ for the conventional method, and compare with two values of L' (2 and 4).

To visualise the spectral performance, a simulation is performed, with $L = 8$, to evaluate filtered spectra using each window function, for 802.11p symbols. The spectral responses are plotted in Fig. 5, where the same OFDM signal as in Fig. 4 has been filtered by the FIR interpolation filters, and compared to the SEMs. In the figure, the filtered spectra obtained by using Kaiser, Hamming, Hanning, Blackman, and Chebyshev windows are compared (denoted using the abbreviations in Table 2). In each case, two prominent auxiliary peaks, visible beside the main spectrum, are the biggest impediments to satisfying the SEM criteria. In detail, the Blackman filtered spectrum slightly exceeds the class A limits, whereas the remaining filters are able to meet the requirements of classes A and B but not of classes C and D. In fact, none of the filters can achieve class C or D compliance. Hence, given the effective guard interval of 802.11p, FIR filtering clearly does not provide a solution.

The simulation results show that the common filtering methods used at interpolated baseband are not even close to meeting the strict SEM requirements of 802.11p. Although not shown here, this is of course equally true of the more stringent 802.11af SEM. This result implies that 802.11p and 802.11af implementations must rely on sharp front end RF and analogue filtering, which typically results in an increased total system cost and reduced power efficiency, unless an alternative is found.

4. Proposed method and results

The discussions above have revealed that the main challenge to conforming to strict SEMs is the narrow frequency guard which

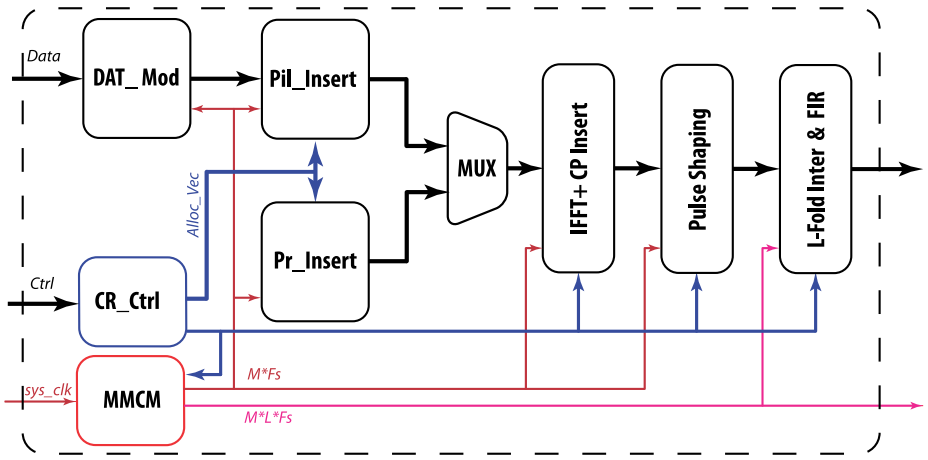

Fig. 6. CR architecture for adaptive OFDM spectral leakage shaping.

must accommodate a very sharp filter transition between pass and stop bands, with high stop-band attenuation. We first proposed a method of achieving this for 802.11p in [11]. In this section, we briefly explain the method before building upon its foundation to derive a CR architecture for OFDM spectral leakage mitigation which we will then evaluate for both 802.11p and 802.11af.

4.1. New spectral leakage filtering method

In a conventional approach, pulse shaping is only employed with small roll-off factors. This is because large roll-off factors involve longer filters, reducing the effective guard interval. Given the narrow frequency guard of the OFDM spectrum for the new standards, and the amount left after accounting for the effects of CIR and matching filters, pulse shaping under such constraints is unable to cancel the image spectrum: in fact, even if the entire guard interval was to be used, this may be insufficient for the very stringent class D SEM in 802.11p, and the SEM of 802.11af. Thus our new method takes a different approach. Instead of using a large proportion of the guard interval for FIR filtering, we allow the pulse shaping to occupy a significant portion of the guard space, with large roll-off factors. To obtain the significant spectral leakage reduction necessary, the frequency guard needs to be increased. It thus involves introducing a frequency guard extension technique. Then, given a wider frequency guard, pulse shaping with large roll-off factors can achieve significant side lobe compression of the OFDM signal, and the required transition band for FIR filtering is extended, which means a shorter FIR filter is able to attenuate the image spectrum.

The method involves three steps:

- The IFFT length is multiplied by a factor M, and the sampling frequency similarly increased by a factor M, to maintain the same subcarrier spacing. Given this, the allocation vector is formed to add data symbols at lower sub-carriers that are the same as those in the original IFFT, while the remaining sub-carriers are zero-padded.
- Next, pulse shaping is applied in the normal way, to meet the given SEM constraint.
- Finally, L'-fold interpolation is used to allow simple filtering to remove the image spectrum.

In [11], the three steps were implemented for a fixed solution (i.e. constant M and L'), and shown to meet the SEM requirements for one standard. In this paper, we build a flexible CR architecture which is demonstrated to achieve the SEM requirements for both 802.11p (all classes A, B, C, and D) as well as 802.11af in the UHF band.

4.2. Novel CR filtering architecture

A CR architecture for OFDM implies the agility to handle non-contiguous (NC) transmission of symbols (NC-OFDM) as well as the ability to adapt to different frequency bands, bandwidths and timing synchronisation regimes. For the purposes of this paper, a CR architecture is developed which combines transmission of NC-OFDM symbols with switched sampling frequency, supporting both 802.11p and 802.11af. In particular, the architecture adaptively extends the frequency guard as required, and performs both pulse shaping and FIR interpolation filtering to meet the most strict SEM requirements of both standards. It should be understood that this CR architecture is designed to demonstrate compliance with the more difficult standards: it could trivially be de-rated to the much less stringent 802.11a and 802.11ac parent standards.

The proposed CR-based transmitter architecture structure is presented in Fig. 6, as implemented on a *Xilinx Virtex-6 FPGA* for experimental purposes.

As can be seen, the architecture consists of the following baseband sub-modules:

- *Pil_Insert* flexibly inserts data symbols and pilots from the data modulator, *DAT_Mod*, into an OFDM symbol according to the current allocation vector (*Alloc_Vec*).
- *Pre_Insert* inserts the preamble symbol, specified by the standard, before sending the OFDM symbols of a data frame. The preamble symbol is used for synchronisation at the receiver.
- *IFFT+CPInsert* performs IFFT modulation and adds the CP to each OFDM symbol. This module is implemented using a Xilinx FFT IP core that is configured to allow flexible reconfiguration of IFFT length and CP insertion.
- *PulseShaping* performs pulse shaping with a smoothing function for which the roll-off factor can be changed from small (for relaxed spectral shaping) to large (for more stringent spectral shaping). A block diagram of this module's implementation is provided in Fig. 7. The coefficients of the smoothing functions are pre-loaded into memory. They are multiplied by the modulated samples in the time domain. The *suffix buf* buffers the suffix smoothing of the previous symbol to add to the prefix smoothing (recall the pulse shaping operation performed on OFDM symbols in Fig. 1).
- *L-FoldInter&FIR* performs L'-fold interpolation, with L' being controllable on a symbol-by-symbol basis. After interpolation, the FIR block is used to filter out the image spectrum. This

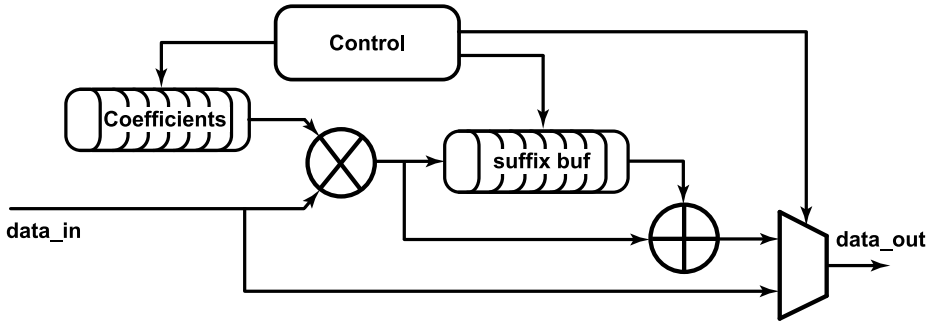

Fig. 7. A block diagram of the Pulse Shaping implementation.

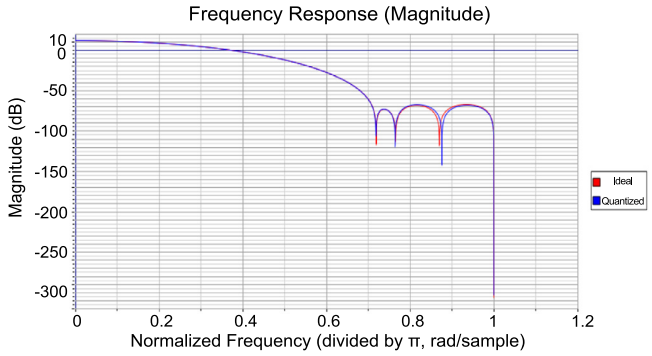

Fig. 8. The frequency response of the implemented FIR interpolation filter. (For interpretation of the colours in this figure, the reader is referred to the web version of this article.)

block is implemented using the Xilinx FIR compiler IP core. Fig. 8 shows the frequency response of the FIR implementation for 802.11p. *Ideal* denotes the performance in theory with high number precision, whereas *Quantized* plots the performance achieved using 16-bit coefficient precision.

In addition, for the CR architecture, the cognitive control sub-module (*CR_Ctrl*) is used to modify sub-module parameters to match SEM requirements imposed by the higher layers (i.e. it adjusts timing, bandwidth, frequency band and SEM requirements). The mixed-mode clock manager (*MMCM*) is another integrated IP core used to manage the sampling clock (F_s), which is set dynamically according to the filter performance requirements and operating frequency band.

The *MMCM* also allows the transmitter to specify a reduced degree of filtering (i.e. degree of spectral leakage shaping) when transmission power is reduced, since transmit power reduction naturally reduces ICI as a consequence, thus less filtering will be needed. This is particularly important for lower power operating modes in which a lower sampling frequency, less filtering complexity, and reduced transmission power all contribute to energy savings.

Compare this with the 802.11p prototype presented in [32], which was adopted for direct device-to-device communication between smartphones. That prototype was able to adaptively increase transmission power to extend communication range. However, the system was based on an 802.11a hardware solution and baseband, and did not investigate the increased spectral leakage when the transmitted signal was amplified to increase range (at which point it would not be likely to meet the 802.11p SEM requirement).

By contrast, the method proposed and implemented in this paper, is able to apply a more stringent SEM filter when transmission power is increased such that ICI exceeds a given threshold. In particular, *CR_Ctrl* is invoked to change the IFFT length to M times the original IFFT, while *Alloc_Vec* extends the frequency guard and *MMCM* increases F_s according to the required IFFT length. Moreover, *CR_Ctrl* changes *PulseShaping* to use a large roll-off factor, reduces the L-fold interpolation (since $L' \times M$ is constant) and shortens the FIR length to meet the more stringent SEMs. On the other hand, when a device and access point are in closer proximity, the transmission power can be reduced such that the spectral leakage is small, and thus filtering can be relaxed. In this case, *CR_Ctrl* is invoked to change the IFFT length back to the original, and employ *PulseShaping* with a small roll-off factor. Moreover, *L-FoldInter&FIR* switches back to a normal range in order to reduce the amount of computation.

Table 3
Hardware usage for spectral shaping.

Method	Max freq	Module	Slices	DSPs	BRAMs
FixedArch	242 MHz	IFFT+CPInsert	613	18	1
		PulseShaping	36	0	0
		L-FoldInter&FIR	139	10	0
FlexArch	223 MHz	IFFT+CPInsert	1282	34	1
		PulseShaping	41	2	0
		L-FoldInter&FIR	189	12	0

In order to provide the flexibility for dynamically shaping spectral leakage, the processing modules (i.e. *IFFT+CPInsert*, *PulseShaping*, *L-FoldInter&FIR*) are implemented with the ability to switch operating mode at run time. This in turn involves an increase in hardware resources compared to a fixed implementation. Table 3 compares the hardware requirements of the modules for the proposed flexible method, *FlexArch*, and a fixed architecture, *FixedArch* (IFFT length and FIR length are fixed), and the maximum clock frequency achievable for two architectures. It should be noted that the additional computation needed for signal processing in the baseband (which uses low cost, low power components), can be more than compensated for by relaxing the specification of the RF front-end design, since the analogue filtering requirements are so much less strict. *FixedArch* has a maximum frequency that is slightly higher than *FlexArch*, but both architectures significantly exceed the requirement (80 MHz).

The following subsections present the application of the proposed CR architecture to performing stringent filtering to achieve the SEM specifications of both 802.11p and 802.11af respectively.

4.3. Configuration and performance evaluation for 802.11p

Based on the signal model and environmental factors discussed in Section 2, the CIR length is assumed to not exceed 600 ns. Therefore, the effective guard interval, equivalent to the length of 10 samples of the original CP, i.e., $10 \times 100 = 1000$ ns, is used for the pulse shaping and FIR filter. By choosing a DAC sampling frequency of 80 MHz, the sampling frequency for 802.11p is in-

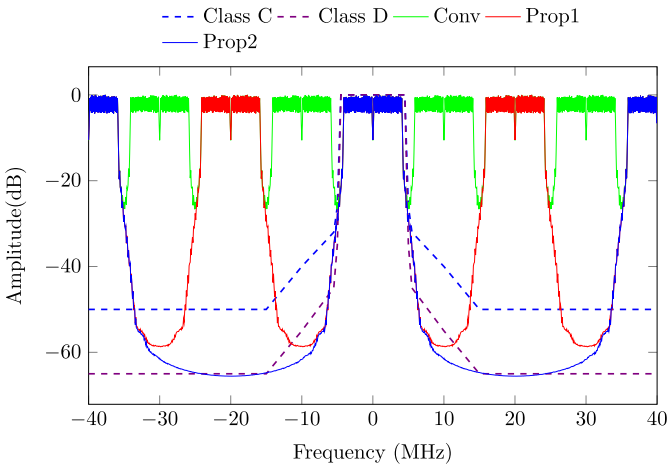

Fig. 9. Spectrum of 802.11p signal of the proposed CR architecture after interpolation. (For interpretation of the colours in this figure, the reader is referred to the web version of this article.)

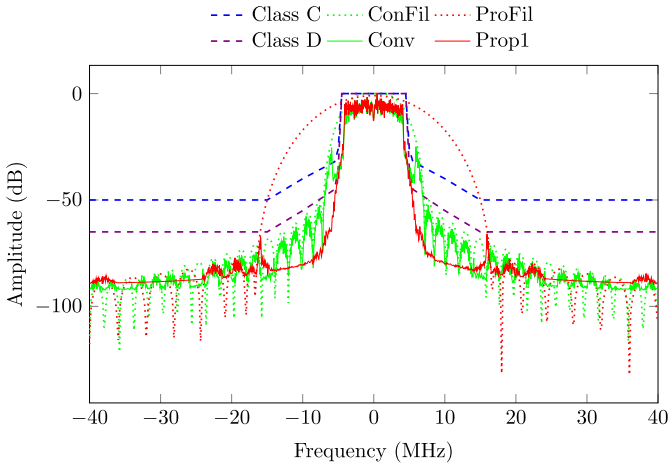

Fig. 10. Spectrum of 802.11p signal using option *Prop1* with 19th order FIR filtering. (For interpretation of the colours in this figure, the reader is referred to the web version of this article.)

Table 4
The coefficient set for the FIR filters of the proposed method.

Filter	Coefficients
PFR1	−0.00059, −0.00368, −0.00597, 0.00615, 0.05827, 0.17805, 0.37511, 0.62262, 0.85664, 1, 1, 0.85664, 0.62262, 0.37511, 0.17805, 0.05827, 0.00615, −0.00597, −0.00368, −0.00059
PFR2	−0.00061, −0.00544, 0.02798, 0.22399, 0.62835, 1, 1, 0.62835, 0.22399, 0.02798, −0.00544, −0.00061

creased by 8 times ($L'.M = 8$) over the original nominal rate of 10 MHz. Based on this configuration, two optional systems, denoted as *Prop1* and *Prop2*, will now be explored for 802.11p:

Prop1 doubles the size of the IFFT, i.e., $M = 2$, which means doubling the sampling frequency to extend the frequency guard, after which 4-fold interpolation, i.e., $L' = 4$, is required to obtain a sampling frequency of 80 MHz.

Prop2 quadruples the size of the IFFT, i.e., $M = 4$; Then applies 2-fold interpolation, i.e., $L' = 2$ to achieve the 80 MHz sampling frequency.

Based on the results in Section 3.1, $p_2(m)$ is employed with $\beta N_T = 5 \times M$. i.e. equivalent to the length of 5 samples of the original CP, i.e., 500 ns. It should be noted that, after extending the frequency guard, the number of samples in the symbol, including CP, is increased M times. Fig. 9 plots the shaped spectrum of the proposed method after interpolation in the baseband, at a sampling frequency of 80 MHz. The original spectrum denoted *Conv*, and the specifications for classes C and D are also shown. It can be seen that the main spectrum for *Prop1* and *Prop2* both almost satisfy class D. However the image spectrum of *Prop1* is present at ±20 MHz and ±40 MHz whereas *Prop2* has an image spectrum at ±40 MHz only.

A simpler, shorter-length FIR filter is then needed to cancel the image spectra, since they lie much further away in frequency than for the original approach, *Conv*. The remaining guard interval for the transmitter filter and matched filter is 500 ns. Therefore, the maximum impulse response available for the image rejection FIR filter is 250 ns, which is equivalent to $2.5 \times M.L'$ samples at the 80 MHz sampling frequency.

FIR filters *PFR1*, *PFR2* are designed for *Prop1* and *Prop2* respectively, using a Kaiser window, with filter coefficients given in Table 4.

For *Prop1*, since the frequency guard is still relatively narrow, an FIR filter with an impulse length of 20 samples is required to cancel the image spectrum. Fig. 10 shows the result of spectrum

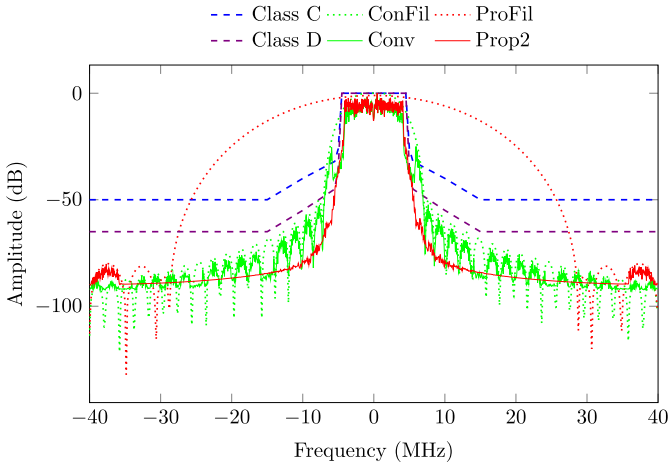

Fig. 11. Spectrum of 802.11p signal for *Prop2* with 11th order FIR filtering. (For interpretation of the colours in this figure, the reader is referred to the web version of this article.)

filtering for *Prop1*, with the original OFDM spectrum (*Conv*) and SEMs for classes C and D overlaid. *PFR1* and *CFR* are the frequency response of the filters used for *Prop1* and *Conv*, respectively.

It can be seen that there are still two small peaks caused by the image spectrum, but these are compressed by the FIR filter to meet the class D requirement. Some distortion is also noticeable in the main spectrum due to the effects of the FIR filter.

Prop2 has a wider frequency guard compared to *Prop1* and thus its FIR filter only requires a length of 12 samples to cancel the image spectrum. A remaining effective guard interval of 200 ns is reserved.

Similarly, Fig. 11 plots the result of this degree of spectral filtering for *Prop2* and its filter response *PFR2* and with respect to the class C and D SEMs. Clearly the image spectrum of *Prop2* can be cancelled by a short-length FIR filter, while suffering less distortion (rounding) to the main passband.

The simulation results are presented in terms of Signal-to-Mask Ratio (SMR) with respect to class D in Fig. 12. This plot clearly demonstrates that the proposed CR architectures *Prop1*, *Prop2* can meet the class D mask specification, the most stringent of the four 802.11p SEMs. In general, *Prop2* obtains better performance in terms of distortion and effective guard interval compared to *Prop1*, but pays the cost of a higher computational requirement due to the increased IFFT size.

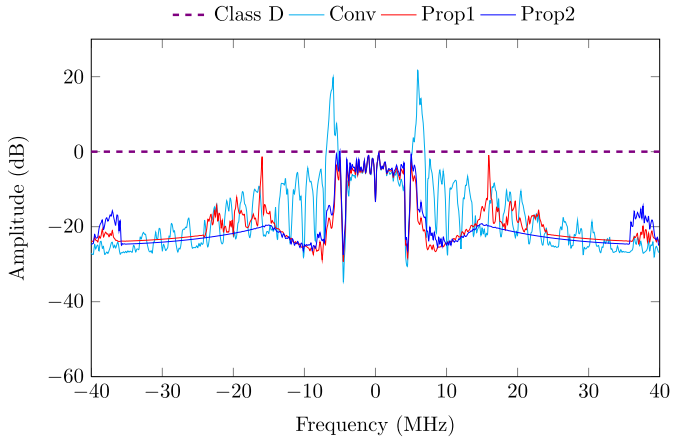

Fig. 12. The Signal-to-Mask Ratio of shaped spectra to the mark of class D. (For interpretation of the colours in this figure, the reader is referred to the web version of this article.)

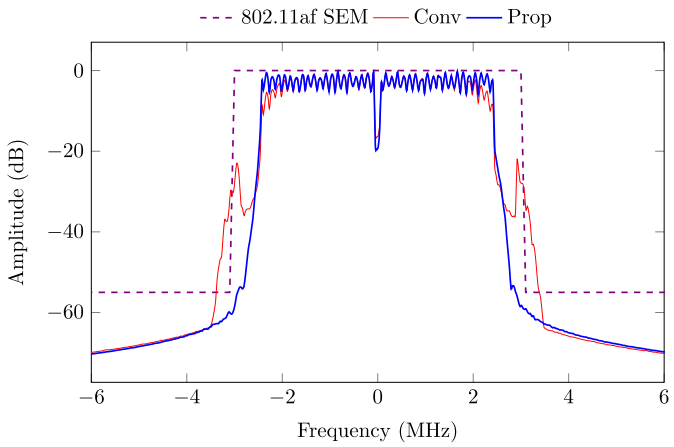

Fig. 13. Spectrum of 802.11af signal using the proposed CR architecture. (For interpretation of the colours in this figure, the reader is referred to the web version of this article.)

4.4. Configuration and performance evaluation for 802.11af

Based on the discussion in Section 2, if the CIR length is assumed to not exceed 1 μs, this is equivalent to 6 samples in the 802.11af CP. Therefore, the effective guard interval, equivalent to a length of 26 samples of the original CP, is available for use by the pulse shaping and FIR filters.

By choosing a DAC sampling frequency of 48 MHz, the output sampling frequency of 802.11af is increased by 8 times ($L'.M = 8$) compared to the original nominal frequency (6 MHz). Simulation results for shaping the spectral leakage of 802.11af are presented here. The proposed method is compared to the conventional approach which makes use of state-of-the-art pulse shaping and FIR filtering. In the conventional approach, pulse shaping uses 2 samples in the CP for a smoothing function, and the length of the FIR filter for cancelling the image spectrum is allowed to extend to 96 ($\frac{26-2}{2} \times 8$) to avoid ISI. Again, the FIR filter is designed using a Kaiser window, with a cut-off frequency set to attempt to compress the signal spectrum to meet the FCC mandated SEM.

Our proposed method quadruples the size of the IFFT (i.e. $M = 4$), to extend the frequency guard. Pulse shaping is configured to employ $p_2(m)$ from Section 3.1, with $\beta N_T = 20 \times M$. That is equivalent to the length of 20 samples of the original CP. Then 2-fold interpolation (i.e. $L' = 2$), is required to obtain the sampling frequency of 48 MHz. The maximum allowed FIR filter length for cancelling the image spectrum without inducing ISI is equivalent to 3 samples of the original CP. Fig. 13 illustrates the results of shaping the spectral leakage for 802.11af using this proposed CR architecture.

Because of the limited length, the band transition of the FIR filter is not narrow enough. This results in the spectrum of the conventional method, *Conv*, exhibiting two side lobes, as well as introducing visible distortion in the main spectrum. Thus, the conventional method is far from able to meet the SEM requirement for 802.11af. One method that might be considered for achieving this is to deactivate the outer sub-carriers (instead, use null-subcarriers). This can extend the frequency guard, but clearly results in a loss of spectral efficiency. Reducing transmission power is also possible, but is similarly unattractive since it would adversely impact range – in fact the power reduction needed to bring the *Conv* transmission within the SEM envelope is not small. For example, the 802.11af prototype hardware in [14] requires the transmitted power to be attenuated by 20 dB to satisfy the SEM specifications.

On the other hand, the spectrum of the proposed CR architecture, denoted in Fig. 13 as *Prop*, comfortably meets the SEM specification without impacting either range or spectral efficiency.

4.5. 802.11af spectral efficiency

Another way of investigating performance is to compute spectral efficiency, given a flexible allocation of subcarriers. In other words to adjust the number of occupied subcarriers until the transmission profile fits within the 802.11af SEM, and using the unoccupied subcarrier space for filter roll off. In the conventional method (Fig. 13), about 35 dBc additional filtering would be needed to suppress the image spectrum at the edge of the channel bandwidth (3 MHz), from −20 dBc, to −55 dBc.

With a 96th order FIR filter as mentioned above for *Conv*, the transition band needed to achieve such suppression is estimated, based on the Kaiser window formula in Table 2, as being 0.83 MHz. This is equivalent to 21 subcarrier spacings which would need to be trimmed from each side of the 802.11af channel. Thus the number of occupied sub-carriers would need to be reduced from the standard 114 subcarriers to below 100 in order to give *Conv* a sufficient guard interval for FIR filtering.

However, the window formula is only an estimate, and hence the system is simulated here to explore further. In this case, the number of sub-carriers is reduced step-wise in pairs, from the edges working inwards, until the SEM is just satisfied. Fig. 14 plots results with 94 and 92 sub-carriers occupied (*Conv_94s* and *Conv_92s*), showing that 92 sub-carriers meets the SEM requirement whereas 94 sub-carriers does not, by a small margin.

Referring back to Fig. 13, a clear frequency gap is evident between the spectrum of the proposed approach and the SEM. This gap could potentially be exploited to pack in several more occupied sub-carriers. We therefore undertake simulations to explore this phenomenon, and find that the proposed method is able to pack in up to 124 employed sub-carriers while still satisfying the SEM. This is also illustrated in Fig. 14 as *Prop_124s*. Compared to the approach of trimming off edge carriers needed by an equivalent transmission power system in order to satisfy the SEM, the proposed approach to CR spectrum shaping increases spectral efficiency by 32%.

This result demonstrates that the proposed CR architecture can not only meet the stringent SEM requirement of 802.11af but is also able to deactivate and reactivate subcarriers selectively, allowing it to adapt in the face of changing operating conditions and requirements to achieve the best spectral efficiency for a given SEM.

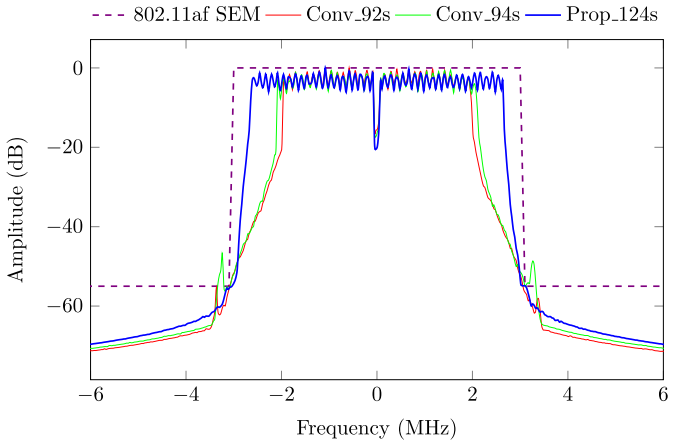

Fig. 14. Fitting filtered spectrum of 802.11af signal to SEMs. (For interpretation of the colours in this figure, the reader is referred to the web version of this article.)

5. Conclusion

This paper has investigated leakage shaping for OFDM-based cognitive radios, presenting an architecture that can meet stringent spectral emission mask (SEM) requirements. In particular, we have considered two relatively new standards, 802.11p and 802.11af, which have physical layers derived largely from existing standards. In both cases, the extended physical layers are scaled to encourage re-use of existing hardware, devices and designs, but the resulting systems are then subject to much more stringent SEMs.

Our previous baseband method for 802.11p relies upon a combination of interpolation, IFFT length adjustment, pulse shaping and FIR image suppression filtering to mitigate against spectral leakage into adjacent channels. In this paper, we extend the fixed method by parameterising and embedding the technique into a flexible and scalable cognitive radio (CR) architecture which we then apply to 802.11af in addition to 802.11p.

The propose architecture can adaptively change the degree of spectral leakage filtering done in baseband in response to changes in transmission power and operating requirement. This allows reduced computation when transmission power is low, but guaranteed SEM performance when transmission power is high, meeting the requirements for both 802.11p and 802.11af, as well as for CR implementation in general. Furthermore, the architecture is a highly agile solution that is capable of adjusting clock rate, bandwidth, and frequency band on a symbol-by-symbol basis.

Simulations show that the proposed architecture can meet the specification of the four 802.11p classes A to D, as well as the stringent FCC-imposed SEM for 802.11af in the UHF band. We also demonstrate the flexible deactivation and reactivation of outlying subcarriers to adapt to changing conditions, and show how this improves spectral efficiency for 802.11af in the TV whitespace band by 32%, compared to equivalent transmission power approaches, which must drop their outermost subcarriers in order to meet SEM requirements.

References

[1] IEEE 802 Standard; Part 11; Amendment 6: Wireless access in vehicular environments, IEEE, Jul. 2010.
[2] W. Vandenberghe, I. Moerman, P. Demeester, Approximation of the IEEE 802.11p standard using commercial off-the-shelf IEEE 802.11a hardware, in: International Conference on ITS Telecommunications, ITST, 2011, pp. 21–26.
[3] J. Fernandez, K. Borries, L. Cheng, B. Kumar, D. Stancil, F. Bai, Performance of the 802.11p physical layer in vehicle-to-vehicle environments, IEEE Trans. Veh. Technol. 61 (1) (2012) 3–14.
[4] D. Jiang, L. Delgrossi, IEEE 802.11p: towards an international standard for wireless access in vehicular environments, in: IEEE Vehicular Technology Conference, VTC, 2008, pp. 2036–2040.
[5] IEEE Standard for wireless access in vehicular environments-multi-channel operations, IEEE, Dec. 2010.
[6] X. Wu, S. Subramanian, R. Guha, R. White, J. Li, K. Lu, A. Bucceri, T. Zhang, Vehicular communications using DSRC: challenges, enhancements, and evolution, IEEE J. Sel. Areas Commun. 31 (9) (2013) 399–408.
[7] D. Lo Iacono, T. Cupaiuolo, Power efficient SDR implementation of IEEE 802.11a/p physical layer, J. Signal Process. Syst. 73 (3) (2013) 281–289.
[8] W.-Y. Lin, M.-W. Li, K.-C. Lan, C.-H. Hsu, A comparison of 802.11a and 802.11p for V-to-I communication: a measurement study, in: Quality, Reliability, Security and Robustness in Heterogeneous Networks, in: Lecture Notes of the Institute for Computer Sciences, Social Informatics and Telecommunications Engineering, vol. 74, Springer, 2012, pp. 559–570.
[9] N. de Almeida, J. Matos, J. Lopes, A front end to vehicular communications, in: IEEE International Conference on Computer as a Tool, EUROCON, 2011, pp. 1–4.
[10] P. Fuxjäger, A. Costantini, D. Valerio, P. Castiglione, G. Zacheo, T. Zemen, F. Ricciato, IEEE 802.11 p transmission using GNURadio, in: Proceedings of the Karlsruhe Workshop on Software Radios, WSR, 2010, pp. 83–86.
[11] T.H. Pham, I.V. McLoughlin, S.A. Fahmy, Shaping spectral leakage for IEEE 802.11p vehicular communications, in: IEEE Vehicular Technology Conference, VTC, May 2014, pp. 1–5.
[12] IEEE 802 Standard; Part 11; Amendment 5: Television White Spaces (TVWS) operation, IEEE, Dec. 2013.
[13] S. Shellhammer, A. Sadek, W. Zhang, Technical challenges for cognitive radio in the TV white space spectrum, in: Information Theory and Applications Workshop, Feb. 2009, pp. 323–333.
[14] Z. Lan, K. Mizutani, G. Villardi, H. Harada, Design and implementation of a Wi-Fi prototype system in TVWS based on IEEE 802.11af, in: IEEE Wireless Communications and Networking Conference, WCNC, April 2013, pp. 750–755.
[15] C. Masse, A direct-conversion transmitter for WiMAX and WiBro applications, RF Des. 29 (1) (2006) 42–46.
[16] Y.-M. Chen, I.-Y. Kuo, Design of lowpass filter for digital down converter in OFDM receivers, in: International Conference on Wireless Networks, Communications and Mobile Computing, vol. 2, June 2005, pp. 1094–1099.
[17] J. Dowle, S.H. Kuo, K. Mehrotra, I.V. McLoughlin, FPGA-based MIMO and space–time processing platform, EURASIP J. Appl. Signal Process. 34653 (Jan. 2006) 1–14.
[18] M. Faulkner, The effect of filtering on the performance of OFDM systems, IEEE Trans. Veh. Technol. 49 (5) (Sep. 2000) 1877–1884.
[19] K.N. Le, Insights on ICI and its effects on performance of OFDM systems, Digit. Signal Process. 18 (6) (2008) 876–884.
[20] A. Selim, L. Doyle, Practical out-of-band interference reduction for OFDM systems, in: Proc. IEEE Global Communications Conference, GLOBECOM, Dec. 2013, pp. 3510–3515.
[21] A. Selim, B. Ozgul, L. Doyle, Efficient cyclic prefix reconstruction for shaped OFDM systems without cyclic prefix, in: IEEE Global Communications Conference, GLOBECOM 2010, Dec. 2010, pp. 1–5.
[22] R. Saxena, H.D. Joshi, Performance improvement in an OFDM system with MBH combinational pulse shape, Digit. Signal Process. 23 (1) (2013) 314–321.
[23] I. Macaluso, B. Ozgul, T. Forde, P. Sutton, L. Doyle, Spectrum and energy efficient block edge mask-compliant waveforms for dynamic environments, IEEE J. Sel. Areas Commun. 32 (2) (February 2014) 307–321.
[24] T. Forde, L. Doyle, B. Ozgul, Dynamic Block-Edge Masks (BEMs) for dynamic Spectrum Emission Masks (SEMs), in: IEEE Symposium on New Frontiers in Dynamic Spectrum, April 2010, pp. 1–10.
[25] P. Kryszkiewicz, H. Bogucka, Dynamic determination of spectrum emission masks in the varying cognitive radio environment, in: IEEE International Conference on Communications, ICC, June 2013, pp. 2733–2737.
[26] G. Acosta-Marum, M.-A. Ingram, Six time and frequency selective empirical channel models for vehicular wireless LANs, IEEE Veh. Technol. Mag. 2 (4) (2007) 4–11.
[27] I. Sen, D. Matolak, Vehicle–vehicle channel models for the 5-GHz band, IEEE Trans. Intell. Transp. Syst. 9 (2) (2008) 235–245.
[28] E. Bala, J. Li, R. Yang, Shaping spectral leakage: a novel low-complexity transceiver architecture for cognitive radio, IEEE Veh. Technol. Mag. 8 (3) (2013) 38–46.
[29] D. Castanheira, A. Gameiro, Novel windowing scheme for cognitive OFDM systems, IEEE Wirel. Commun. Lett. 2 (3) (2013) 251–254.
[30] B. Farhang-Boroujeny, Signal Processing Techniques for Software Radios, Lulu Publishing House, 2008.
[31] R.J. Kapadia, Digital Filters Theory, Application and Design of Modern Filters, Wiley VCH, 2012.
[32] P. Choi, J. Gao, N. Ramanathan, M. Mao, S. Xu, C.-C. Boon, S.A. Fahmy, L.-S. Peh, A case for leveraging 802.11p for direct phone-to-phone communications, in: Proceedings of the International Symposium on Low Power Electronics and Design, 2014, pp. 207–212.

Thinh H. Pham received his B.S. degree in Electrical Electronic Engineering at Ho Chi Minh City, University of Technology, Viet Nam, and MSc. degree in Embedded Systems Engineering at the University of Leeds,

UK, in 2007 and 2010, respectively. He completed his Ph.D. in the joint Nanyang Technological University – Technische Universitat Munchen program in Singapore in 2015 while working as a Research Associate with the TUM CREATE Centre for Electromobility, Singapore. He is now a Lecturer at Ho Chi Minh City, University of Technology, Viet Nam.

Suhaib A. Fahmy received the M.Eng. degree in information systems engineering and the Ph.D. degree in electrical and electronic engineering from Imperial College London, UK, in 2003 and 2007, respectively. He was a Research Fellow with Trinity College Dublin, Ireland, and Visiting Research Engineer with Xilinx Research Labs, Dublin, from 2007 to 2009. From 2009 to 2015 he was an Assistant Professor with the School of Computer Engineering at Nanyang Technological University, Singapore. He joined the School of Engineering at the University of Warwick, UK, in 2015. His research interests centre around reconfigurable computing and hardware design, across the domains of wireless communications, computer vision, automotive systems, and, more recently, accelerator systems. Dr. Fahmy was a recipient of the best paper award at the IEEE Conference on Field Programmable Technology in 2012, and the IBM Faculty Award in 2013. He is a Senior Member of the IEEE and ACM.

Ian Vince McLoughlin splits his career between the electronics R&D industry and academia, based in five countries on three continents. He became a Chartered Engineer in 1998, a Senior Member of IEEE in 2004, a D'Ingenieur Europeen (EU) in 2008, and a Fellow of the IET in 2013. He is currently professor in the School of Computing at the University of Kent, UK and is head of the Medway school. He was previously a professor in the University of Science and Technology of China (USTC) and before that worked in Nanyang Technological University, Singapore. His Ph.D. in electronic and electrical engineering was completed at the University of Birmingham, UK, in 1997.